J. Chem. Sci. Vol. 128, No. 12, December 2016, pp. 1879–1885. © Indian Academy of Sciences.
DOI 10.1007/s12039-016-1192-z

Self-supported porous Cobalt Oxide Nanowires with enhanced Electrocatalytic performance toward Oxygen evolution reaction

HAN XIA[a,b], ZHEN PENG[a,*], CUNCAI L V[b], YAOXING ZHAO[b], JINHUI HAO[b] and ZHIPENG HUANG[b,*]

[a]School of Materials Science and Engineering, Jiangsu University, Zhenjiang 212013, People's Republic of China
[b]Functional Molecular Materials Research Centre, Scientific Research Academy, Jiangsu University, Zhenjiang 212013, P. R. China
e-mail: peng@ujs.edu.cn; zphuang@ujs.edu.cn

MS received 5 July 2016; revised 11 September 2016; accepted 4 October 2016

Abstract. Development of hybrid electrocatalysts with high activity and good stability is crucial for oxygen evolution reaction (OER) of water electrocatalysis. In this work, cobalt oxide (Co_3O_4) nanowires loaded on carbon fiber paper (CFP) were synthesized *via* hydrothermal method and annealing. The as-synthesized Co_3O_4 nanowires exhibit an enhanced catalytic activity with low onset overpotential (1.52 V vs. RHE) and a small overpotential of 330 mV for a current density of 10 mA cm^{-2} with a Tafel slope of 60 mV·dec^{-1}. In addition, the Co_3O_4 nanowires maintain its electrocatalytic activity for at least 24 h in basic media. The enhanced performance of Co_3O_4 nanowires/CFP can be attributed to the high conductivity of CFP, the synergistic effect of Co_3O_4 and carbon, and high porosity of the nanowire. This study will open new possibilities for exploring water electrocatalysis.

Keywords. Electrocatalyst; oxygen evolution reaction; Co_3O_4 nanowires; carbon fiber paper; over potential.

1. Introduction

With the increase in population and the rapid socio-economic development, energy requirements become more intensive.[1–4] The conventional fossil fuels belong to non-renewable energy, and they emit plenty of harmful gases.[1] The exploitation of sustainable and environmental energy is highly desirable.[2,3] Electricity-driven water splitting is a promising way to solve the energy problem, having attracted already a broad interest.[5,6]

Water electrolysis can be divided into two half reactions: hydrogen evolution reaction (HER) and oxygen evolution reaction (OER).[7] The OER is a 4-electron process to form only one oxygen molecule.[8] Because the OER needs a larger overpotential to complete electrical catalysis process, the sluggish kinetics of the OER becomes a major limitation in efficient water electrolysis.[7–10] Based on this, a lot of research has been focused on preparing low cost OER catalyst with high efficiency, and long-term stability.[11] The main aim is to reduce the OER overpotential. Among many reported metal oxides, RuO_2, IrO_2, and PtO_2 are regarded as the most active OER electrocatalysts, their scarcity and high cost greatly limit their large scale applications.[12,13] Thus, there is considerable interest in developing OER catalysts based on earth-abundant metals such as Co, Fe and Ni, the oxides of which exhibit efficient electrochemical activity in the OER.[3,11,14] Currently, these non-noble transition-metal-based OER catalysts are usually obtained from precursor solutions of metal ions, and prepared as a thin films on two-dimensional planar substrates by common methods such as electrodeposition, dip-coating, sputtering, etc.[3,15] Although performance has improved significantly, the structural, mechanical and electrical contact between catalyst and substrates should be optimized to further strengthen the stability and activity of the catalyst layer.[3,6,10,11]

Fabricating an ideal structure of catalysts is a direct and efficient approach to further optimize the OER performance.[16] It has been demonstrated that a vertically aligned nanowire array of active components grown directly on current collectors can be considered as a new kind of highly effective electrodes.[17] Definitely, this type of structure provides a tight coupling between catalyst and current collector and a short electron transport pathway, facilitating electron transport and electrolyte diffusion. Moreover, nanowire array significantly promotes the escape of as-formed gas

*For correspondence

bubbles from the surface of electrode, offering a stable and fast current increase.[3,16,17] It is well-known that this structure was widely used for HER. Nevertheless, the application of nanowire array as an electrocatalyst for the OER has been rarely documented.[13]

In this work, we demonstrated the construction of Co_3O_4 nanowires (Co_3O_4NW) on carbon fiber paper (CFP) and its prominent electrocatalytic activity in the OER. The CFP-Co_3O_4 NW has an onset potential of 1.52 V vs. reversible hydrogen electrode (RHE) and a fast current increase, affording a current density of 10 mA cm^{-2} with overpotential as small as 330 mV. The performance is superb compared to that of other nanostructures with similar composition, Co precursor nanowire ($Co(OH)(CO_3)_{0.5}$NW) and Co_3O_4 nanorod (Co_3O_4NR), and that of other transition metal oxides. Meanwhile, the CFP-Co_3O_4NW showed prominent stability at a high reaction rate for a long time and faradaic efficiency of 92% during water oxidation. The facile synthesis and prominent performance render the CFP-Co_3O_4NW promising material for a wide range of applications.

2. Experimental

2.1 *Reagents*

Cobalt nitrate hexahydrate ($Co(NO_3)_2{\cdot}6H_2O$, AR) and urea ($CO(NH_2)_2$, AR) were purchased from Sinopharm Chemical Reagent Co., Ltd. Ammonium fluoride (NH_4F, GR) was purchased from shanghai Aladdin Industrial Corporation. Commercial CFP was purchased from Shanghai Hesen. All the reagents were used as received without further purification. Deionized water (resistivity: 18.2 MΩ cm) was used throughout our experiments.

2.2 *Materials Synthesis*

CFP was cut into pieces of 2×6 cm^2 and then cleaned by sequential sonication in acetone, H_2SO_4 solution, and deionized water each for 10 min to form a clean and hydrophilic surface for the hydrothermal growth. $Co(NO_3)_2{\cdot}6H_2O$ (0.87 g), $CO(NH_2)_2$ (0.90 g) and NH_4F (0.22 g) were dissolved in 80 mL water. The solution was transferred to a 100 mL Teflon-lined stainless steel autoclave loaded with a piece of CFP. The autoclave was then put in a constant temperature oven at 120°C for 7 h. After cooling down to room temperature, the sample was taken out and washed ultrasonically with water several times. Finally the sample was dried at 80°C for 2 h.[18,19]

The pink $Co(OH)(CO_3)_{0.5}$ NW samples were annealed at 250°C in air for 2 h with a ramping rate of 2°C min^{-1}. After cooling down to room temperature, the ash black Co_3O_4 was formed on CFP.[16,20]

Co_3O_4 nanorods were prepared by annealing the $Co(OH)(CO_3)_{0.5}$ powder collected after hydrothermal growth at 250°C in air for 2 h.[20,21]

Preparation of Co_3O_4 nanorod-loaded electrodes: 6 mg Co_3O_4 nanorod and 40 μL 5 wt.% Nafion solution were dispersed in 500 μL water/ethanol (v:v = 4:1) by 60 min sonication to form a catalyst ink. Then 45 μL catalyst ink was loaded on CFP with a loading mass of 1.35 mg cm^{-2}.

2.3 *Characterization*

The samples were characterized by X-ray diffraction (XRD, RIGAKU D/Max-2550 with Cu Kα radiation), scanning electron microscopy (SEM, FEI SIRION), and transmission electron microscopy (TEM, JEOLJEM-2010F).

2.4 *Electrochemical Measurements*

The electrochemical measurements were carried out by an electrochemistry workstation (CHI 614D) in a three-electrode cell containing aqueous KOH solution (1 M). The catalyst loaded on CFP was used as the working electrode, a mercury/mercury oxide electrode (MOE) as the reference electrode, and a high-surface-area Pt mesh as the counter electrode. A porous glass frit separated the chambers of working electrode and the counter electrode. The reversible hydrogen evolution potential (RHE) was determined by the open circuit potential of a clean Pt electrode in the solution of interest bubbled with H_2 (99.999%). The potential measured *vs.* MOE was referenced to that *versus* RHE by adding 0.936 V. The overpotential (η) of OER was computed through η (V)=E(RHE) − 1.23 V.[22]

Linear sweep voltammetry (LSV) curves were measured at a scan rate of 5 mV·S^{-1}. The curves were corrected for the iR drop, where 'I' is the current at relevant potential and R is the uncompensated cell resistance estimated by current-interrupt method. The Tafel slope was figured from the LSV curve by fitting experimental data to the equation $\eta = a + b \log j$, where η is iR-corrected potential, 'a' is Tafel constant, 'b' is Tafel slope, and 'j' is current density. Electrochemistry impendence spectroscopy (EIS) were measured at 1.6 mV vs. RHE in the frequency range of 10^{-2} to 10^6 Hz. The volume of O_2 evolved during potentiostatic electrolysis experiment was monitored by water displacement method, and the details have been described in our previous publication.[23]

3. Results and Discussion

Figure 1 gives the scheme for the whole preparation process. The CFP was chosen here as the conductive substrate. Its relatively rough surface and high porosity structure may contribute to augment the active surface area.[19] The synthesis of Co_3O_4NWs on CFP contains two steps: the synthesis of $Co(OH)(CO_3)_{0.5}$NWs on CFP using a hydrothermal method, and the annealing of the above sample in air. By the hydrothermal process, $Co(OH)(CO_3)_{0.5}$ NWs were successfully grown on CFP, and reliable contacts were formed between the NWs and CFP.[19] After annealing, $Co(OH)(CO_3)_{0.5}$ was oxidized to Co_3O_4, and the morphology feature of self-supported nanowire array was still maintained. The Co_3O_4 NR (not shown in the schematic) comes from cobalt carbonate hydroxide $Co(OH)(CO_3)_{0.5}$ collected from hydrothermal solution after heat-treatment.

The X-ray diffraction (XRD) pattern was recorded to determine the component of products. The XRD pattern of the sample resulted from hydrothermal growth is given in Figure 2a, and the pattern is matching well with that of the $Co(OH)(CO_3)_{0.5}$ (JCPDS PDF48-0058).[19] Figure 2b gives the XRD pattern of Co_3O_4 with different morphologies, including Co_3O_4 NWs and Co_3O_4 NR. Both of them can be well-indexed to the cubic spinel Co_3O_4 (JCPDS 80-1534), and no detectable impurity phase could be found. It is therefore suggested that all precursors were successfully converted into Co_3O_4. Owing to Co_3O_4 NWs and $Co(OH)(CO_3)_{0.5}$ NWs growth on the CFP, peaks corresponding to the CFP were labeled by rhomboids.

The morphologies of NWs of $Co(OH)(CO_3)_{0.5}$ and Co_3O_4 supported by CFP were examined with the scanning electron microscopy (SEM). As shown in Figures 3a and 3b, $Co(OH)(CO_3)_{0.5}$ NWs grew homogeneously on the surface of CFP. The diameter of the $Co(OH)(CO_3)_{0.5}$ nanowires is about 168 nm and their length is up to around 9.5 μm. After annealed at 250°C in air, the $Co(OH)(CO_3)_{0.5}$ NWs were completely converted into Co_3O_4 NWs without any morphology variation (Figures 2c and 2d). It was proved that annealing did not damage the shape of the structure. Nevertheless, the diameter of nanowires is decreased to 123 nm. This may be attributed to gas (e.g., CO_2, H_2O) escaping from the nanowire during the annealing process.[10] Different magnification SEM of $Co(OH)(CO_3)_{0.5}$ NWs and Co_3O_4 NWs were provided in Figure S1 (see Supplementary Information). The typical loading amount of the Co_3O_4 NWs on the CFP was measured to be 1.35 mg cm^{-2}. Figure S2 (Supplementary Information) shows a typical SEM image of Co_3O_4 NR. A rod-like morphology can be seen in the low magnification SEM image (Figure S2a, Supplementary Information), but the length is irregular. A high magnification SEM image (Figure S2b, Supplementary Information) shows that these nanorods have a rough surface.

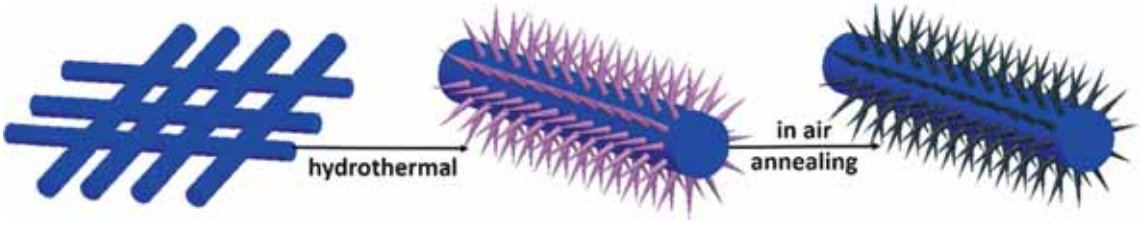

Figure 1. Schematic illustration of the synthesis of Co_3O_4 NWs on CFP.

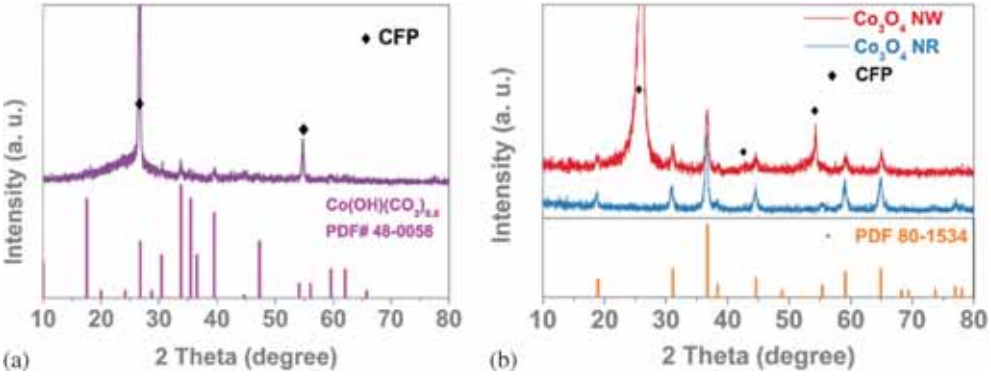

Figure 2. (a) XRD pattern of CFP-$Co(OH)(CO_3)_{0.5}$NW. (b) XRD patterns of CFP-Co_3O_4 NW (red line) and Co_3O_4NR (cyan line).

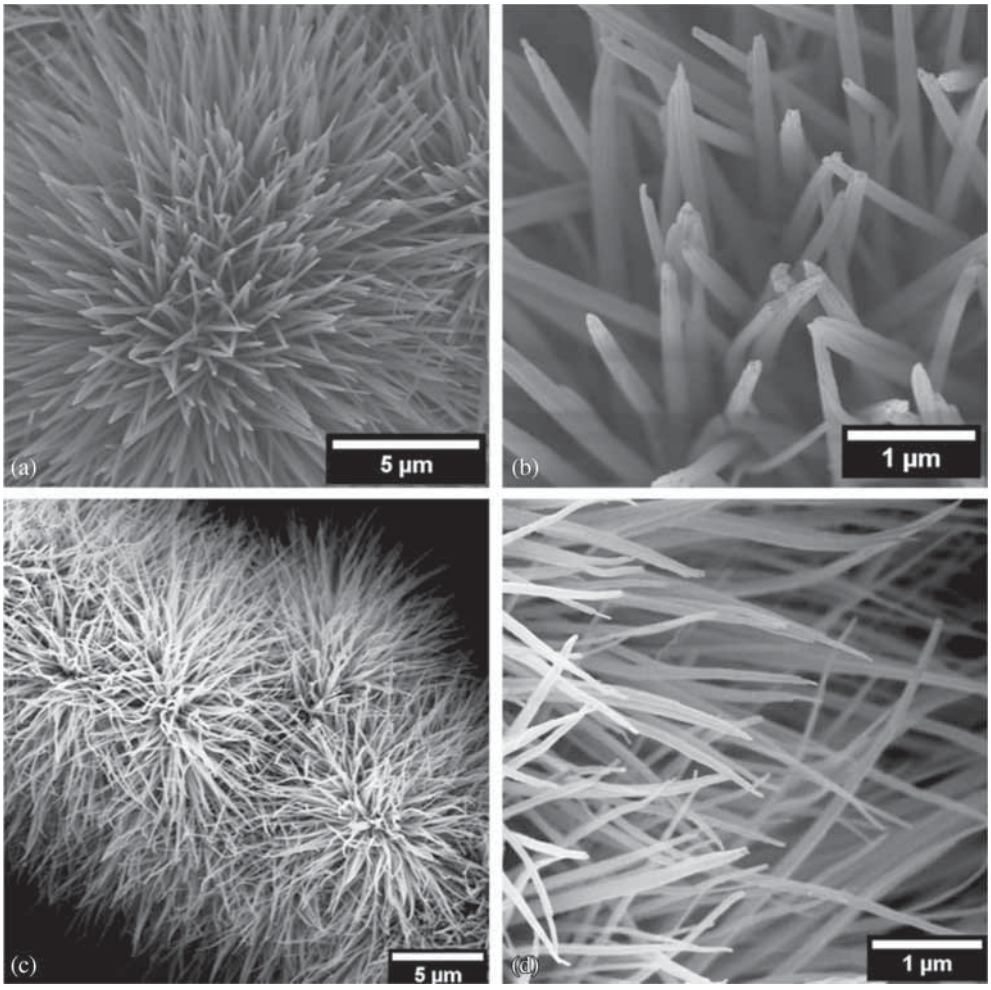

Figure 3. The SEM image of $Co(OH)(CO_3)_{0.5}$ on CFP ((a) and (b)) and Co_3O_4 nanowires ((c) and (d)) array at a calcination ramping rate of 2°C per min.

The microstructure of Co_3O_4 nanowires was examined by TEM experiments (Figure 4). Figure 4a shows a low magnification TEM image of Co_3O_4 nanowires desquamated from the CFP substrate. The morphology of Co_3O_4 shown in the picture corresponds to that revealed by the SEM experiment. TEM image with larger magnification (Figure 4b) shows that the Co_3O_4 nanowires are composed of closely connected nanoparticles. The diameter of the nanoparticles is about 12.7 nm. A lot of clearance formed between nanoparticles greatly enlarge the area of the interface. The high resolution TEM (HRTEM) image of a Co_3O_4 nanowire is given in Figure 4c. It is illustrated that the Co_3O_4 nanowire is poly-crystalline. The obvious lattice fringe can be found in its corresponding fast Fourier transform (FFT) pattern which is shown in the inset of Figure 4c. The pattern can be indexed to the [1 $\bar{3}$0] zone axis diffraction pattern of cubic phase Co_3O_4 ($1/d_{OA}$, $= d_{(31-1)} = 0.24$ nm, $1/d_{OB} = d_{(311)} = 0.24$ nm, $1/d_{OC} = d_{(002)} = 0.41$ nm, $\angle AOB = 35.1°$, and $\angle BOC = 72.4°$).

To demonstrate the activity of Co for OER, the polarization curves was measured (Figure 5). The catalytic activity of the $Co(OH)(CO_3)_{0.5}$ NWs grown on CFP electrodes was studied initially by linear sweep voltammetry (LSV) in a standard three-electrode cell. The overpotential required for a current density of 10 mA cm^{-2} (η_{10}) is 355 mV for $Co(OH)(CO_3)_{0.5}$ NW. When it was completely converted to Co_3O_4 NW, the overpotential decreased to 330 mV. The OER activity ofCo_3O_4 NR deposited on CFP was examined with the same mass loading as that of CFP-Co_3O_4 NW. It required an overpotential of 370 mV to achieve the current density of 10 mA cm^{-2}. Meanwhile, the CFP-Co_3O_4 NW had a low onsetpotential at 1.52 V vs. RHE. The small oxidative peak between 1.4 and 1.5 V vs. RHE is associated with the formation of CoOOH.[24–27] It is worth mentioning that lowering of overpotential to 330 mV is needed to afford benchmark current density of 10 mA cm^{-2}; it is superior to previous reports such as Ni-doped Co_3O_4 (530 mV)[16], Au@Co_3O_4 (386 mV)[28], NiCo LDH(367 mV)[29] and Co-P (345 mV)[30], and so on.

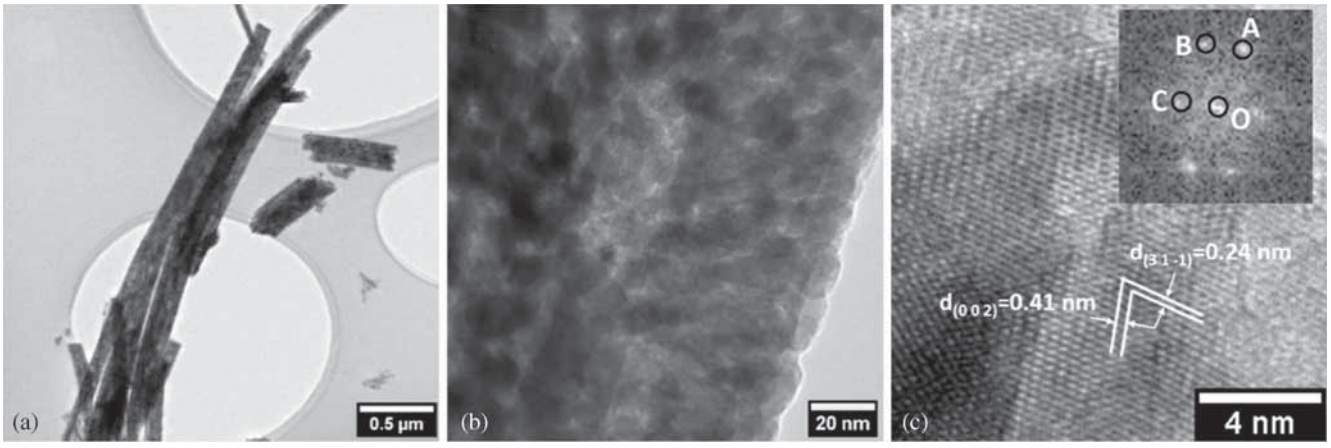

Figure 4. ((a) and (b)) TEM images of Co_3O_4 NW. (c) HRTEM image of Co_3O_4 NW. The inset is the FFT pattern of the lattice.

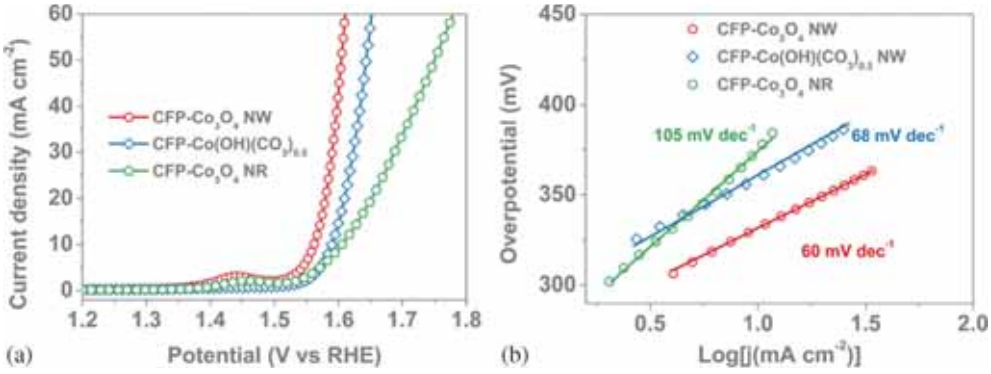

Figure 5. (a) Polarization curves of the $Co(OH)(CO_3)_{0.5}$ NW@CFP (green line), Co_3O_4 NW@CFP (red line) and Co_3O_4 NR@CFP (cyan line). (b) Tafel plots of samples (red line: Co_3O_4 NW@CFP, green line: $Co(OH)(CO_3)_{0.5}$ NW@CFP, cyan line: Co_3O_4 NR@CFP).

A list of performance of various non-precious metal oxides in the OER can be found in Table S1 (Supplementary Information). To gain more insight on the OER activity, Tafel plots derived from polarization curves were constructed (Figure 5b). The resulting Tafel slope of CFP-Co_3O_4 NW was 60 mV·dec^{-1}, which is smaller than that of CFP-$Co(OH)(CO_3)_{0.5}$NW (68 mV·dec^{-1}) and CFP-Co_3O_4NR (105 mV·dec^{-1}), indicating that the CFP-Co_3O_4NW exhibited better OER activity.[13]

Electrochemically active surface area (ECSA) should play an important role in the high electrocatalytic performance, and it was derived from the specific capacitance measured by CV scans (Figure S3 in Supplementary Information).[31] The potential range of the CV scans was selected at 1.1–1.2 V vs. RHE which did not include obvious electrochemical features corresponding to faradaic current. As a result, the dependence of the current on the scan rate in this region for both electrodes was linear, which was consistent with capacitive charging behavior.[32] The specific capacitance of the CFP-Co_3O_4 NW, CFP-$Co(OH)(CO_3)_{0.5}$ NW and CFP-Co_3O_4 NR were measured to be 39.6, 34.6 and 10.9 mF·cm^{-2}, respectively (Figure S3d), and the corresponding ECSA is 990.0, 865.0, and 272.5 cm^2_{ECSA} (detailed discussion is given in Supplementary Information), suggesting that the ECSA of the nanowire is much larger than that of the CFP-Co_3O_4 NR. It is demonstrated that the nanowire structure could increase the number of electrochemically active sites for the OER.[33,34]

To further understand the surface area of the catalyst, the Brunauer–Emmett–Teller (BET) experiment was conducted. From BET measurements, the specific surface area of Co_3O_4 NW was estimated as 34.644 m^2 g^{-1}, which is relatively larger than Co_3O_4 NR (31.886 m^2 g^{-1}). The nitrogen adsorption-desorption isotherm is shown in Figure S4 (Supplementary Information). The BET of Co_3O_4 NR and Co_3O_4 NW have slight differences but the ECSA of CFP-Co_3O_4 NR is much smaller than that of CFP-Co_3O_4 NW. The smaller ECSA of CFP-Co_3O_4 NR correlates with its larger electron transport resistance, in comparison with that of CFP-Co_3O_4 NW. In this case, the electrons cannot be delivered to every

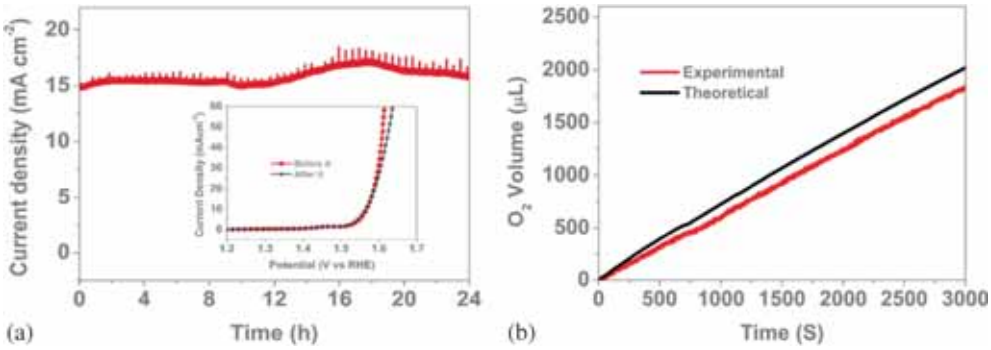

Figure 6. (a) The relationship of current density and time in a potentiostatic electrolysis experiment (applied potential: 1.57 V vs. RHE). The inset shows the LSV before and after electrolysis. (b) The comparison of theoretical and experimental volumes of the generated O_2 in a potentiostatic electrolysis experiment (applied potential: 1.7 V vs. RHE, without iR correction).

Co_3O_4 NR, and some Co_3O_4 NR will therefore be inert in HER. The BET and ECSA measurements demonstrate clearly that the growth of Co_3O_4 NW directly on the surface of CFP is beneficial for the electron transport from electrode to catalyst and inside the catalyst, and is important to make every Co_3O_4 NW active in the case of high catalyst loading.

High durability is important for the practical application of OER catalyst.[35,36] Potentiostatic electrolysis was used to evaluate the stability of the CFP-Co_3O_4 NW. No degradation of current density was found after 24 h of potentiostatic electrolysis (Figure 6a). However, the overpotential required to drive a current density of 60 mA cm^{-2} (η_{60}) increases from 370 to 400 mV after the long time electrolysis test (the inset plot in Figure 6a). The decay of η_{60} is about 8%. The faradaic efficiency of the Co_3O_4 NW during O_2 evolution was evaluated by the comparison of the volume of generated gas and the theoretical volume in the potentiostatic electrolysis measurement. Before the test, the electrolyte was aerated (O_2) for 4 h. The plots of theoretical and experimental volumes of the generated oxygen versus the experimental time are shown in Figure 6b. During electrolysis for 3000 s, 32 coulombs of charge were passed and 1.86 mL of O_2 was evolved, which gave a Faradaic yield of 92%.

4. Conclusions

In summary, porous Co_3O_4 nanowire arrays were successfully grown on CFP through hydrothermal and calcination, and it exhibited superior OER activity compared to the CFP-$Co(OH)(CO_3)_{0.5}$ NW and CFP-Co_3O_4 NR. The CFP-Co_3O_4 NW has an onset potential of 10.52 V vs. RHE and only a small overpotential of 330 mV is needed to afford a benchmark current density (η_{10}). Moreover, the electrode is stable for 24 h at high current density and 92% faradaic efficiency. The porous three-dimensional architecture should play an essential role in enhancing the OER activity. It can offer an even higher surface area, while the conductivity can be well preserved.

Supplementary Information (SI)

Additional information about characterization of CFP-$Co(OH)(CO_3)_{0.5}$ and Co_3O_4 NR using SEM (Figures S1, S2), performance of representative electrocatalysts for water oxidation (Table S1), equivalent circuit used to fit the EIS data (Figure S3), values of elements in the equivalent circuit (Table S2), cyclic voltammograms (Figures S4), and calculation of electrochemical active surface area are given in the supporting information. Supplementary Information is available at www.ias.ac.in/chemsci.

Acknowledgements

This study was financially supported by the National Natural Science Foundation of China (61006049), Jiangsu Province (2011-XCL-019 and 2013-479), the Natural Science Foundation of Jiangsu (BK20131252), Natural Science Fund for Colleges and Universities in Jiangsu Province (Grant No. 16KJB430005) and Ordinary University Graduate Student Research Innovation Projects of Jiangsu Province (SJLX15_0487).

References

1. Chow J 2003 *Sci.* **302** 1528
2. Cook T R, Dogutan D K, Reece S Y, Surendranath Y, Teets T S and Nocera D G 2010 *Chem. Rev.* **110** 6474
3. Xu W W, Lu Z Y, Lei X D, Li Y P and Sun X M 2014 *Phys. Chem. Chem. Phys.* **16** 20402

4. Wang J, Zhong H X, Wang Z L, Meng F L and Zhang X B 2016 *ACS Nano* **10** 2342
5. Walter M G, Warren E L, McKone J R, Boettcher S W, Xi M Q, Santori E A and Lewis N S 2010 *Chem. Rev.* **110** 6446
6. Wang J, Zhong H X, Qin Y L and Zhang X B 2013 *Angew. Chem. Int. Ed. Engl.* **52** 5248
7. McCrory C C, Jung S, Ferrer I M, Chatman S M, Peters J C and Jaramillo T F 2015 *J. Am. Chem. Soc.* **137** 4347
8. Markoulaki I V, Papadas I T, Kornarakis I and Armatas G 2015 *Nanomaterials* **5** 1971
9. Long X, Li J, Xiao S, Yan K, Wang Z, Chen H and Yang S 2014 *Angew. Chem. Int. Ed.* **53** 7584
10. Sharifi T, Gracia-Espino E, Jia X, Sandström R and Wågberg T 2015 *ACS Appl. Mater. Interfaces* **7** 28148
11. Zou X X, Silva R, Goswami A, Sathe B and Asef T 2013 *Chem. Commun.* **49** 7522
12. Koza J A, He Z, Miller A S and Switzer J A 2012 *Chem. Mater.* **24** 3567
13. Chen R, Wang H Y, Miao J W, Yang H B and Liu B 2015 *Nano Energy* **11** 333
14. Yu X, Zhang M, Yuan W and Shi G 2015 *J. Mater. Chem. A* **3** 6921
15. Wang H F, Tang C, Zhu X and Zhang Q 2016 *J. Mater. Chem. A* **4** 3379
16. Lu B, Cao D, Wang P, Wang G and Gao Y 2011 *Int. J. Hydrogen Energy* **36** 72
17. Ma T Y, Dai S, Jaroniec M and Qiao S Z 2014 *J. Am. Chem. Soc.* **136** 13925
18. Faber M S, Dziedzic R, Lukowski M A, Kaiser N S, Ding Q and Jin S 2014 *J. Am. Chem. Soc.* **136** 10053
19. Wang K, Zhou C J, Xi D, Shi Z Q, He C, Xia H Y, Liu G W and Qiao G J 2015 *Nano Energy* **18** 1
20. Rakhi R B, Chen W, Hedhili M N, Cha D and Alshareef H N 2014 *ACS Appl. Mater. Interfaces* **6** 4196
21. Zhou X, Shen X, Xia Z, Zhang Z, Li J, Ma Y and Qu Y 2015 *ACS Appl. Mater. Interfaces* **7** 20322
22. Liu T, Liang Y, Liu Q, Sun X, He Y and Asiri A M 2015 *Electrochem. Commun.* **60** 92
23. Huang Z P, Chen Z Z, Chen Z B, Lv C C, Humphrey M G and Zhang C 2014 *Nano Energy* **9** 373
24. Sayeed M A, Herd T and O' Mullane A P 2016 *J. Mater. Chem. A* **4** 991
25. Tahir M, Mahmood N, Zhang X, Mahmood T, Butt F K, Aslam I, Tanveer M, Idrees F, Khalid S, Shakir I, Yan Y, Zou J, Cao C and Hou Y 2015 *Nano Res.* **8** 3725
26. Wu L, Li Q, Wu C H, Zhu H, Mendoza-Garcia A, Shen B and Guo J 2015 *J. Am. Chem. Soc.* **137** 7071
27. Mao S, Wen Z, Huang T, Hou Y and Chen J 2014 *Energy Environ. Sci.* **7** 609
28. Zhuang Z, Sheng W and Yan Y 2014 *Adv. Mater.* **26** 3950
29. Liang H, Meng F, Caban-Acevedo M, Li L, Forticaux A, Xiu L, Wang Z and Jin S 2015 *Nano Lett.* **15** 1421
30. Jiang N, You B, Sheng M and Sun Y 2015 *Angew. Chem. Int. Ed. Engl.* **54** 6251
31. Song F and Hu X 2014 *Nat. Commun.* **5** 1
32. Kibsgaard J and Jaramillo T F 2014 *Angew. Chem. Int. Ed. Engl.* **53** 14433
33. Zhao Y F, Chen S Q, Sun B, Su D W, Huang X D, Liu H, Yan Y M, Sun K N and Wang G X 2015 *SCI REP-UK* **7629** 1
34. Yan X D, Li K X, Lyu L, Song F, He J, Niu D, Liu L, Hu X and Chen X B 2016 *ACS Appl. Mater. Interfaces* **8** 3028
35. Zhang X L, Zhang J B and Wang K 2015 *ACS Appl. Mater. Interfaces* **7** 20745
36. Hu H, Guan B Y, Xia B Y and Lou X W 2015 *J. Am. Chem. Soc.* **137** 5590